

Received:
01 February 2019

Revised:
18 June 2020

Accepted:
23 June 2020

<https://doi.org/10.1259/bjr.20190121>

Cite this article as:

Buzan MTA, Wetscherek A, Rank CM, Kreuter M, Heussel CP, Kachelrieß M, et al. Delayed contrast dynamics as marker of regional impairment in pulmonary fibrosis using 5D MRI - a pilot study. *Br J Radiol* 2020; **93**: 20190121.

FULL PAPER

Delayed contrast dynamics as marker of regional impairment in pulmonary fibrosis using 5D MRI - a pilot study

^{1,2,3,4}MARIA TA BUZAN, MD, PhD, ^{5,6}ANDREAS WETSCHEREK, PhD, ⁵CHRISTOPHER M RANK, PhD, ^{3,7}MICHAEL KREUTER, MD, PhD, ^{1,3,7}CLAUS PETER HEUSSEL, MD, PhD, ⁵MARC KACHELRIEß, PhD and ^{1,8,9}JULIEN DINKEL, MD, PhD

¹Department of Diagnostic and Interventional Radiology with Nuclear Medicine, Thoraxklinik at Heidelberg University Hospital, Heidelberg, Germany

²Department of Pneumology, Iuliu Hatieganu University of Medicine and Pharmacy, Cluj-Napoca, Romania

³Translational Lung Research Center Heidelberg (TLRC), Member of the German Center for Lung Research (DZL), Heidelberg, Germany

⁴Addenbrooke's Hospital, Cambridge University Hospitals NHS Foundation Trust, Cambridge, United Kingdom

⁵Medical Physics in Radiology, German Cancer Research Center (DKFZ), Heidelberg, Germany

⁶Joint Department of Physics at The Institute of Cancer Research and The Royal Marsden NHS Foundation Trust, London, United Kingdom

⁷Center for Rare and Interstitial Lung Diseases, Pneumology and respiratory critical care medicine, Thoraxklinik, Heidelberg University Hospital, Heidelberg, Germany

⁸Institute for Clinical Radiology, Ludwig-Maximilians-University Hospital Munich, Munich, Germany

⁹Comprehensive Pneumology Center Munich (CPC-M), Member of the German Center for Lung Research (DZL), Munich, Germany

Address correspondence to: Dr Andreas Wetscherek

E-mail: andreas.wetscherek@icr.ac.uk

Objective: To analyse delayed contrast dynamics of fibrotic lesions in interstitial lung disease (ILD) using five dimensional (5D) MRI and to correlate contrast dynamics with disease severity.

Methods: 20 patients (mean age: 71 years; M:F, 13:7), with chronic fibrosing ILD: $n = 12$ idiopathic pulmonary fibrosis (IPF) and $n = 8$ non-IPF, underwent thin-section multislice CT as part of the standard diagnostic workup and additionally MRI of the lung. 2 min after contrast injection, a radial gradient echo sequence with golden-angle spacing was acquired during 5 min of free-breathing, followed by 5D image reconstruction. Disease was categorized as severe or non-severe according to CT morphological regional severity. For each patient, 10 lesions were analysed.

Results: IPF lesions showed later peak enhancement compared to non-IPF (severe: $p = 0.01$, non-severe: $p = 0.003$). Severe lesions showed later peak enhancement compared to non-severe lesions, in non-IPF ($p = 0.04$),

but not in IPF ($p = 0.35$). There was a tendency towards higher accumulation and washout rates in IPF compared to non-IPF in non-severe disease. Severe lesions had lower washout rate than non-severe ones in both IPF ($p = 0.003$) and non-IPF ($p = 0.005$). Continuous contrast agent accumulation, without washout, was found only in IPF lesions.

Conclusions: Contrast agent dynamics are influenced by type and severity of pulmonary fibrosis, which might enable a more thorough characterisation of disease burden. The regional impairment is of particular interest in the context of antifibrotic treatments and was characterised using a non-invasive, non-irradiating, free-breathing method.

Advances in knowledge: Delayed contrast enhancement patterns allow the assessment of regional lung impairment which could represent different disease stages or phenotypes in ILD.

INTRODUCTION

Chronic fibrotic interstitial lung diseases (ILDs) make up a group of progressive disorders that impair the space between the epithelial and endothelial basement membranes by various degrees of inflammation and fibrosis.¹ Pulmonary function testing (PFT) reveals restrictive impairment with reduced lung volumes and

decreased diffusing capacity. Fibrotic ILDs typically carry a poor prognosis, with often limited therapeutic options.² In Europe and USA, two new drugs were cleared recently for the treatment of patients with idiopathic pulmonary fibrosis (IPF).^{3,4} However, antifibrotic therapies still lack reliable metrics to assess therapeutic response and

disease progression, in particular regarding the development and severity of perivascular fibrosis.

30 years ago, McFadden et al were first to suggest a potential role of MRI in the assessment of patients with ILD.⁵ Although an inherent feature of MRI is high soft tissue contrast, contrast-enhanced studies are needed for a more precise assessment. Results of time-intensity curve analysis indicate that inflammation-predominant lesions show fast time to peak, while fibrotic lesions show delayed enhancement.⁶

We hypothesise that the same principle may be applied to further characterise fibrotic lesions of different severity. Recently, a novel motion compensated image reconstruction technique was proposed, which allows for obtaining 4D (four-dimensional) MR images (three-dimensional image volumes for different respiratory phases) of high image quality for morphological assessment,⁷ which can be employed to quantify regional lung volumes.⁸

Standard motion mitigation strategies, such as breath-hold acquisition or gating, have limitations in temporal resolution, signal-to-noise ratio, artefact level, or demand inappropriately long acquisition times.⁷ Studies have previously reported T1 estimation errors when patients were not able to maintain breath-hold. These problems may be minimised by applying a robust sequence, with acquisition in free breathing, which provides excellent image quality and allows for regional analysis of tissue dynamics and lung ventilation.^{7,8} Furthermore, it allows for measurements in any respiratory phase and at any time point within the scanning interval.

In the present study, we aim to analyse the contrast agent accumulation patterns of fibrotic lesions in chronic ILD using a 5D MRI reconstruction of radial gradient echo data acquired in free-breathing. In this context, the term 5D refers to three spatial and two temporal dimensions, extending the concept of 4D MRI to several time points after contrast injection. Moreover, a correlation between the late enhancement dynamics and disease severity will be assessed for a more accurate definition of regional lung function impairment.

METHODS AND MATERIALS

Patients

Patients with chronic fibrotic ILD were examined in a referral tertiary-care university hospital. This prospective study included 20 consecutive patients, recruited over 4 months according to their upcoming clinic appointment, with diagnosis of stable lung fibrosis, made by multidisciplinary clinicroadiologic-pathologic consensus as recommended by current guidelines,⁹ who underwent MRI of the lung. The study cohort included 13 males and 7 females, with a median and interquartile range (IQR) age of 71 [61-73] years.

As part of the standard diagnostic protocol, all patients underwent PFTs and thin-section multislice CT (TSMS-CT). MRI was performed as part of a prospective study to evaluate the contribution of MRI in the assessment of chronic ILD and received

approval from the institutional review board at Thoraxklinik at Heidelberg University Hospital (clearance number S-318/2013). Informed consent was obtained from each patient before the examination.

Computed tomography imaging

All TSMS-CT examinations were performed using a 64-multislice CT system (Somatom Definition AS, Siemens Medical Systems, Erlangen, Germany). Non-contrast scans were obtained from the lung apex to the upper abdomen, during breath-holding at end inspiratory phase. The helical scan protocol applied included: 64 × 0.6 mm collimation, 1.5 pitch, 0.33 s/rotation, 300–330 mm field of view, 512 × 512 matrix, care-dose 4D with a reference of 120 kV and 70 mAs. Reconstructions of all images were performed as contiguous slices of 1.0 mm thickness by means of a standard iterative algorithm (I40) and a lung iterative algorithm (I70).

Magnetic resonance imaging

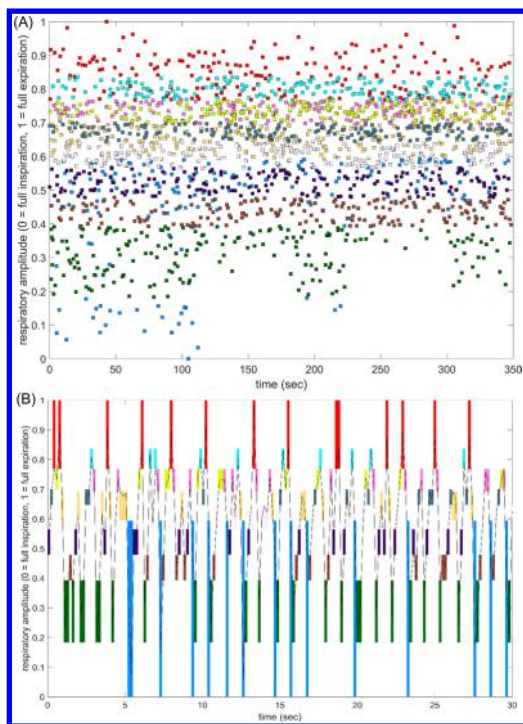
Data acquisition

MRI data were acquired on a 1.5 T clinical whole-body MRI scanner (MAGNETOM Aera, Siemens Healthcare, Erlangen, Germany). A weight-based full dose contrast injection (0.07 mmol/kg patient weight, at 5 ml s⁻¹ injection rate) of gadobutrol was administered. 2 min after contrast injection, a vendor-provided volumetric radiofrequency-spoiled gradient echo sequence with radial stack-of-stars sampling (radial-GRE) and golden angle spacing^{10,11} was performed: slice orientation: sagittal, field-of-view: 385 × 385 × 300 mm, voxel size: 1.5 × 1.5 × 5.0 mm, TR/TE = 3.77/1.69 ms, flip angle: 12°, readout bandwidth = 490 Hz/px. Spectrally selective fat suppression was performed before acquisition of each k-space plane and a partial Fourier factor of 6/8 was used along the Cartesian-encoded dimension in combination with 33% slice oversampling and an acquired slice resolution of 8.33 mm. A total of 2035 radial planes were acquired over a total acquisition time of 350 s. Patients were advised to breathe normally.

5D image reconstruction

Self-gating refers to the use of a motion surrogate, which is derived directly from the acquired MRI data and does not require external devices, such as a respiratory belt, nor separate acquisition of a dedicated navigator signal. We performed respiratory self-gating in MATLAB (MATLAB Release 2015a, The MathWorks, Inc., Natick, MA) based on the magnitude of the k-space center,¹² where the first seven radial planes were excluded to account for the MRI signal reaching a steady-state. Principal component analysis was performed to combine signals from different receiver coils and partitions into one breathing surrogate¹³ and a linear correction based on the exhale peaks of the surrogate signal was performed to account for drifts, e.g. due to contrast agent washout. The remaining 2028 radial planes were sorted by the amplitude of the self-gating signal to determine the end-expiration phase first. Starting from end-expiration, the spokes were sorted based on the amplitude of the breathing signal into a total of 11 overlapping respiratory bins covering the complete breathing cycle and distinguishing between inspiration and expiration (Figure 1 for details).

Figure 1. (A) Representative self-gating signal for the duration of the acquisition. Respiratory states were defined such that the same amount of time is spent in each state. Each colour represents an individual respiratory bin. Note that inspiratory and expiratory states corresponding to the same amplitude of the signal are distinguished, causing a visual overlap of the bins. The deepest inhalatory state is reached primarily at the beginning of the measurement. The end-expiratory phases are most reproducible and exhibit the least amount of motion blurring. Note that the amplitude of the self-gating signal is not directly related to a spatial position. (B) First 30 s of the self-gating signal showing the assignment to respiratory bins using the same colours as in (A). Extent of each bin along the amplitude axis is indicated by a coloured rectangle. Each bin contains the same amount of data when measured over the whole duration of the acquisition.



The radial MRI data were then further assigned to 5 overlapping time-steps (separated by 58.1 s each), resulting in 676 spoke planes each and an average of 122.9 radial spokes per image. After coil sensitivity profiles were jointly estimated for the whole data set,¹⁴ 4D images (11 respiratory phases) were reconstructed separately for each time-step using an in-house developed C++ implementation of the recently published joint motion-compensated high-dimensional total variation algorithm.⁷ In this study, only the end-expiratory phase was used for evaluation, which exhibited the lowest intraphase variation and was least affected by changes in the breathing pattern of the patients (Figure 1A) or blurring in the deepest inhalatory state due to the larger motion range (Figure 1B).

Data analysis and statistics

From the PFTs, we recorded the forced vital capacity and diffusing capacity of lung for carbon monoxide for further analysis.

The morphological severity of lung fibrosis was assessed at TSMS-CT at a regional level by a thoracic radiologist with more than 5 years of experience. Regions with dorsobasal localisation were considered as morphologically severe fibrosis, if honeycombing or reticulation with advanced lung volume loss and architectural distortion was present; and, respectively, non-severe fibrosis, if reticulation or ground glass opacities, with mild/minimal architectural distortion was observed. Architectural distortion was defined based on visual average degree of traction bronchiectasis and bronchiolectasis within the areas of fibrosis. We use the Fleischner Society nomenclature to define honeycombing, reticulation and ground glass lesions.¹⁵ The terms *lesion* and *region* are used interchangeably throughout this manuscript to reflect the diffuse nature of fibrotic lung disease.

On the reconstructed images from the radial MRI acquisition, for each case, 10 regions of interest (in 5 consecutive slices for each lung), were selected corresponding to the lesions defined at TSMS-CT. The acquisition of MRI images in sagittal orientation allowed us to identify the corresponding regions on reference TSMS-CT sagittal reformats, as patients suffering from lung fibrosis cannot achieve deep inspiration, respectively a large displacement of the diaphragm.¹⁶ Further, the analysis performed on contrast-enhanced images with high image quality⁷ facilitated easy identification of anatomical landmarks, such as blood vessels. The availability of 5D MRI enabled identification of the corresponding regions in expiration by tracking them through the respiratory cycle.

To assess the accumulation and washout characteristics for each fibrotic region, changes in signal intensity over the course of the radial MRI acquisition were evaluated at each time step. For each region, the signal intensity was normalised on the average signal intensity at the different time points. The following quantitative parameters were evaluated: time point at which the signal intensity peaked and rates for accumulation and washout of the contrast agent. The rates represent the signal change in percent per minute and were obtained by linear least squares fitting of the data between peak value and first (accumulation), respectively last time point (washout). If the maximum signal intensity was observed at two subsequent time points, then the peak enhancement was considered in the middle of those two time points. For documentation, signal change maps were calculated by pixelwise fitting using ImageJ 1.50b software (U.S. National Institutes of Health, Bethesda, Maryland, USA).

Data analysis were performed using R statistical software version 2.15.1 (R Foundation for Statistical Computing, Vienna, Austria). Categorical data were expressed as absolute values and percentages. Fishers' exact test was applied to verify the differences of frequency for qualitative variables between the groups. Continuous variables were expressed as median and IQR. The Wilcoxon rank-sum test was used to determine differences between groups of quantitative data. All probability values were two-sided, with a significance level of 0.05.

Table 1. General difference between the IPF and non-IPF groups

Criteria	IPF Median [IQR]	Non-IPF Median [IQR]	p-value
Age (years)	72 [69-73]	62 [58-73]	0.2*
Sex (M:F)	10:2	3:5	0.06**
FVC (%)	83 [60-91]	76 [51-94]	0.7*
DLCO (%)	40 [31-47]	48 [45-51]	0.1*
TSMS-CT-MRI interval (days)	0 [0-86]	4 [0-64]	0.7*
Contrast-scan interval (s)	116 [115-126]	123 [120-126]	0.2*

DLCO, diffusing capacity of lung for carbon monoxide; FVC, forced vital capacity; IPF, idiopathic pulmonary fibrosis; IQR, interquartile range; Non-IPF, Idiopathic nonspecific interstitial pneumonia, connective tissue disease-related nonspecific interstitial pneumonia; TSMS, thin-section multislice.

* from Wilcoxon rank-sum test

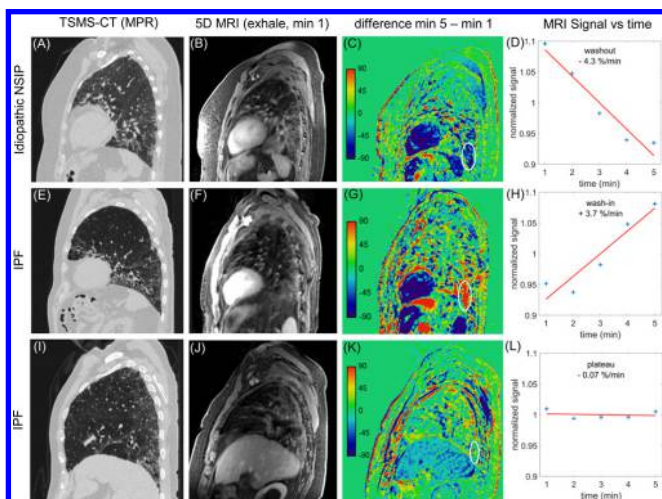
** from Fisher exact test

RESULTS

The final diagnosis was IPF in 12 cases and non-IPF in 8 cases: idiopathic nonspecific interstitial pneumonia (NSIP) in 4 cases, connective tissue disease-related ILD (NSIP pattern) in another 4 cases.

Most of the patients were scheduled to undergo a CT scan during their clinic appointment with only few patients in which CT was not clinically indicated and the most recent CT was used for

Figure 2. Images (A, E and I) represent thin-section multislice CT sagittal reformats; images (B, F and J) represent the joint MoCo-HDTV reconstruction of the T1 radial-GRE acquisition at the first of the five time points; images (C, G and K) represent maps resulting from the difference between the last time step and the first time step; images (D, H and L) display the signal change over time in the drawn region of interest. Images (A-D) Non-severe fibrosis in idiopathic nonspecific interstitial pneumonia showing predominant washout during the scan interval. Images (E-H) Severe fibrosis in idiopathic pulmonary fibrosis showing continuous accumulation of contrast agent during the 5 min scan. Images (I-L) severe fibrosis in idiopathic pulmonary fibrosis showing constant signal intensity during the whole acquisition time. GRE, gradient echo sequence.



reference. The median and IQR interval between CT and MRI was 1 [0-64] days. The median and IQR interval from contrast reaching the pulmonary artery until the start of the study sequence was 121 [116-126] seconds (approximately 2 min). All reconstructed images were of good quality, allowing for further analysis.

We found no general differences between the IPF and non-IPF groups (Table 1). Regarding regional severity of the analysed fibrotic areas, in IPF, 72 regions were considered severe and 48 regions were considered non-severe disease. In non-IPF, 20 regions were considered severe and 60 regions were considered non-severe disease.

After evaluating the time-dependence of signal intensity changes, we found an overall median contrast agent accumulation rate of 1.5 [0.8-3] percent per minute and a washout rate of -1.5 [-2.5-(-0.6)] percent per minute. The first quartile was used as cut-off value for presence of accumulation and the third quartile for the presence of washout. We found 44/200 (22%) lesions, most of them in one IPF and three non-IPF cases, demonstrating plateau signal intensity, with a rate of signal intensity change between -0.6 and 0.8% per minute. From the remaining lesions, 68/200 (34%), most of them found in 3 IPF and 3 non-IPF cases, presented only washout and no accumulation during the scan interval. In 55/200 (27.5%) lesions, most of them found in 6 IPF cases, we found only accumulation and no washout during the acquisition interval. Representative examples are shown in Figure 2.

Regarding the minute of peak enhancement and the contrast agent accumulation and washout rate, we observed several differences both between IPF and non-IPF ILD groups and between severe and non-severe disease. Detailed results are presented in Tables 2 and 3.

Peak enhancement occurred later in IPF regions (around minute 6 after injection) compared to non-IPF (around minutes 3 and 4), $p < 0.05$, with no difference between severe and non-severe disease. In non-IPF, we found a later time to peak in severe compared to non-severe disease, $p = 0.04$.

Table 2. Minute of peak enhancement after contrast injection considering severity assessed on CT

Disease	IPF ^a	Non-IPF ^b	<i>p</i> -value*
Severe	6 [4–7]	4 [4–5]	0.01
Non-severe	6 [4–7]	3 [4–5]	0.003
<i>p</i> -value*	0.35	0.04	

* From Wilcoxon rank-sum test

^aIdiopathic pulmonary fibrosis

^bIdiopathic nonspecific interstitial pneumonia, connective tissue disease-related nonspecific interstitial pneumonia

There was a tendency towards higher accumulation and washout rates in IPF compared to non-IPF in non-severe disease. Both in IPF and non-IPF, the severe lesions had lower washout rate than non-severe ones, $p < 0.05$. Continuous contrast agent accumulation, without washout, was found only in IPF lesions.

DISCUSSION

Standard motion mitigation strategies, such as breath-hold acquisition or gating, have limitations in temporal resolution, signal-to-noise ratio, artefact level, or demand inappropriately long acquisition times.⁷ Studies have previously reported T1 estimation errors when patients were not able to maintain breath-hold. We were able to minimize these problems by applying a robust sequence, with acquisition in free breathing, which provides excellent image quality and allows for regional analysis of tissue dynamics and lung ventilation.^{7,8} Furthermore, it allows for measurements in any respiratory phase and at any time point within the scanning interval.

To the best of our knowledge, this is the first study to show that the type and severity of fibrosing lung disease influence the dynamics of the contrast agent, allowing for a more accurate definition of regional lung function impairment.

As previously reported at time–intensity curve analysis,⁶ inflammation-predominant lesions have a higher percentage signal intensity in the initial dynamic phase at 1 min, while fibrotic predominant lesions have delayed enhancement, with peak enhancement between minute 3 and minute 9. Our results extend these findings: in IPF, regardless of the disease severity assessed on CT, we found a median peak enhancement at minute 6 after injection, while in non-IPF, this was around minutes 3 and 4, with the delay increasing with severity. Mirsadraee and

co-workers showed that the T1 value of fibrotic and apparently normal lung in IPF patients, 10 min after contrast agent administration, was significantly greater than that of normal lung tissue in the control group, and the T1 of fibrotic lung continued to decrease until 20 min after contrast agent administration.¹⁷ We report 44 lesions with unchanged signal intensity values during the scan interval. When reviewing the CT data, some of these lesions were identified in connective tissue disease-related NSIP and had non-severe appearance at regional CT assessment. We interpreted that in these lesions the peak enhancement was before the acquisition started, and these fibrotic lesions had a fast washout, similar to that of inflammatory lesions. Other lesions presented severe disease at CT regional assessment, and we hypothesise that these advanced fibrotic lesions were only reached by minimal, if any, contrast agent, leading to unchanged signal intensity values during the acquisition interval.

Our study shows that severe non-IPF lesions display later peak enhancement compared to non-severe lesions, $p = 0.04$. The early enhancement pattern of non-severe lesions in NSIP may be due to an increase of neovascularisation through angiogenesis in these lesions. Neovascularisation is increased in early fibrosis and decreased in advanced lesions.¹⁸ On the other hand, in usual interstitial pneumonia—the characteristic histological pattern of IPF, well-capillarised intraluminal lesions are typically not present and severe fibrosis was reported to have lower vascularity in fibroblastic foci.¹⁹ This might explain our findings of late peak enhancement in IPF and early peak enhancement in non-IPF (NSIP pattern).

As contrast agent dynamics are influenced by the severity of fibrosis, we believe at least four patterns are of clinical importance: first, advanced fibrotic lesions tend to have the latest peak enhancement, if at all, and very slow contrast dynamics and those are hypothetically less probable to respond to any antifibrotic treatment; second, some morphological non-severe lesions may present an enhancement similar to the one of severe lesions, probably due to more perivascular fibrosis, and their response to treatment could be rather modest; third, some morphologically severe lesions show an earlier enhancement, more similar to that of non-severe lesions, and here treatment might prevent the progress of perivascular fibrosis. An additional pattern of clinical importance is the rapid wash-in and washout corresponding to active inflammatory lesions⁶ and early fibrosis.

Table 3. Rate of contrast agent accumulation and washout (%/min) considering severity assessed on CT

Disease	Accumulation rate			Wash out rate		
	Non-severe	Severe	<i>p</i> -value*	Non-severe	Severe	<i>p</i> -value*
IPF ^a	2.2 [1.6–4]	2.2 [1.5–3.7]	0.92	–2.5 [–3.9–(–1.9)]	–1.6 [–1.9–(–0.9)]	0.003
Non-IPF ^b	1.4 [1.1–2.5]	2 [1.3–4.2]	0.42	–2.0 [–2.8–(–1.6)]	–1.5 [–1.6–(–1)]	0.005
<i>p</i> -value*	0.07	0.98		0.05	0.63	

IPF, idiopathic pulmonary fibrosis.

* From Wilcoxon rank-sum test

^aIdiopathic pulmonary fibrosis

^bIdiopathic nonspecific interstitial pneumonia, connective tissue disease-related nonspecific interstitial pneumonia

Very similar findings were recently reported using hyperpolarised ^{129}Xe MRI.²⁰ The authors described three distinct patterns of pathologic gas exchange which, in concordance with our results, often co-existed in the same patient and may not correlate with disease severity on CT, particularly in IPF. These patterns include: diffusion impairment with increased barrier uptake and delayed red blood cell transfer; end-stage disease with low barrier uptake and almost no red blood cell transfer; and a high barrier uptake coexisting with preserved red blood cell transfer, corresponding to early fibrotic changes. The authors speculated that novel antifibrotic therapies may achieve a positive response in latter group. However, one drawback of this method is the limited availability of hyperpolarised MRI studies, and considering the wider accessibility of dynamic contrast enhancement, our results might be of clinical and research interest. A ^1H MRI-based alternative is the study of late gadolinium enhancement with a stack-of-spirals technique.²¹ Considering the ultrashort echo times (UTE) achievable with this approach, it could be beneficial for studying contrast-agent dynamics in pulmonary fibrosis, considering the higher signal-to-noise ratio associated with UTE imaging.

Jacob et al²² demonstrated a correlation between the pulmonary vessel volume, lung function and extent of disease which suggests that evaluation of pulmonary vessel volume may have implications for the complex fluid dynamics in fibrotic lesions and may be an important new index when assessing disease severity in patients with IPF. Therefore, it may be of interest to analyse in further studies the relationship between delayed contrast dynamics and pulmonary vessel volume, extent of fibrosis and total and lobar pulmonary volume, respectively. The applied 5D MRI method warrants a volumetric evaluation as it would allow for global analysis of the contrast enhancement pattern and generate maps identifying the different stages and severity of fibrosis.

In Europe, antifibrotic treatment is indicated for patients with mild to moderate IPF (forced vital capacity >50% and a diffusing capacity of lung for carbon monoxide > 30–35%).^{3,23} The general severity classification might be misleading in predicting treatment outcome, moreover considering that PFTs are dependent on patients' compliance and the heterogeneous disease distribution cannot be captured using global metrics. More important, since to date the results of ongoing trials including patients with other fibrotic lung disorders have not been published,⁴ it is currently unknown whether antifibrotic therapies will have an effect on other fibrotic ILDs.³ Here, our method might find further application, since we found differences in accumulation patterns between severe and non-severe disease in non-IPF patients at regional severity level. Follow-up studies have shown only minor structural alterations on CT in the first 6 months after diagnosis,²⁴ despite possible functional and symptomatic deterioration. Our method might be a more sensitive assessment of disease progression at regional level, since additional fibrotic accumulation would influence the contrast agent dynamics. Ultimately, this might enable a strategy for the implementation of personalised medicine to the management of chronic ILD.

Our study has four main limitations. First, our study population is small. This is because the study was designed as a proof of principle

to determine the potential applications of 5D MRI in clinical practice and research trials including patients with IPF and fibrotic NSIP. Further studies are needed to validate our results and possibly extend the findings to other categories of patients. Second, despite that vascular distribution tends to be more homogeneous in expiration,²⁵ because the parenchymal abnormalities in lung fibrosis involve mainly the lower lobes,^{9,24} we measured the contrast dynamics only for dorsal lesions. In supine position with resting respiration, gravity determines an increase in blood volume in the posterior part of each lobe. However, at end-expiration phase, the distribution shifts more towards the ventral parts.²⁵ Future research will assess the influence of supine vs prone positioning on contrast agent accumulation patterns in lung fibrosis. Third, in our study we could not calculate the absolute value of enhancement, as our aim was to characterise the delayed contrast dynamics. With the presented non-irradiating free-breathing method, absolute values could be easily obtained, if the contrast agent is administered within the acquisition interval. At the same time, this would allow the assessment of inflammatory or very early fibrotic areas with peak enhancement in the first minute.⁶ In this study, only the exhalation phase was evaluated to minimise the impact of changes in the respiratory pattern on the accuracy of the measurements. This could also be addressed by incorporating a signal model²⁶ into the joint-HDTV reconstruction, but is beyond the scope of this work. Last, our analysis did not take into consideration the presence of comorbidities such as pulmonary hypertension. This will be subject of further prospective research, since the most accurate diagnostic method for pulmonary hypertension—right heart catheterisation—is not regularly performed in all patients with chronic ILD. Especially in patients with advanced interstitial lung disease, there is a low specificity for determining pulmonary hypertension by measuring the pulmonary artery diameter on CT.²⁷

CONCLUSIONS

The contrast agent dynamics are influenced by the type and severity of lung fibrosis. The results might enable a more thorough characterisation of progressive fibrosing lung disease, of special interest being the regional impairment, particularly in the context of new antifibrotic treatments aiming to decelerate disease progression. We demonstrated that this could be achieved using a non-invasive, non-irradiating, free-breathing method.

FUNDING

This study was partly financed from European Society of Thoracic Imaging 2016 Early Stage Chest Radiology Grants and by ERASMUS+ Program for PhD students.

DISCLOSURE

CP Heussel is a consultant of Pfizer, Boehringer Ingelheim, Gilead, Intermune, and Fresenius; he also received research funding from Siemens, Pfizer, and Boehringer Ingelheim as well as fees for lectures from Gilead, MSD, Pfizer, Intermune, Boehringer Ingelheim, and Novartis.

M Kreuter received a grant from Dietmar Hopp Stiftung; he is a consultant for Intermune and he received fees for lectures and educational presentations from Boehringer Ingelheim and Intermune.

REFERENCES

- Martinez FJ, Flaherty K. Pulmonary function testing in idiopathic interstitial pneumonias. *Proc Am Thorac Soc* 2006; **3**: 315–21. doi: <https://doi.org/10.1513/pats.200602-022TK>
- Nathan SD, Shlobin OA, Weir N, Ahmad S, Kaldjob JM, Battle E, et al. Long-Term course and prognosis of idiopathic pulmonary fibrosis in the new millennium. *Chest* 2011; **140**: 221–9. doi: <https://doi.org/10.1378/chest.10-2572>
- Raghu G, Selman M. Nintedanib and pirfenidone. New antifibrotic treatments indicated for idiopathic pulmonary fibrosis offer hopes and raises questions. *Am J Respir Crit Care Med* 2015; **191**: 252–4. doi: <https://doi.org/10.1164/rccm.201411-2044ED>
- Richeldi L, Varone F, Bergna M, de Andrade J, Falk J, Hallowell R, et al. Pharmacological management of progressive-fibrosing interstitial lung diseases: a review of the current evidence. *Eur Respir Rev* 2018; **27**: 180074. doi: <https://doi.org/10.1183/16000617.0074-2018>
- McFadden RG, Carr TJ, Wood TE. Proton magnetic resonance imaging to stage activity of interstitial lung disease. *Chest* 1987; **92**: 31–9. doi: <https://doi.org/10.1378/chest.92.1.31>
- Yi CA, Lee KS, Han J, Chung MP, Chung MJ, Shin KM. 3-T MRI for differentiating inflammation- and fibrosis-predominant lesions of usual and nonspecific interstitial pneumonia: comparison study with pathologic correlation. *AJR Am J Roentgenol* 2008; **190**: 878–85. doi: <https://doi.org/10.2214/AJR.07.2833>
- Rank CM, Heußer T, Buzan MTA, Wetscherek A, Freitag MT, Dinkel J, et al. 4D respiratory motion-compensated image reconstruction of free-breathing radial Mr data with very high undersampling. *Magn Reson Med* 2017; **77**: 1170–83. doi: <https://doi.org/10.1002/mrm.26206>
- Kolb C, Wetscherek A, Buzan MT, Werner R, Rank CM, Kachelrie M, et al. Regional lung ventilation analysis using temporally resolved magnetic resonance imaging. *J Comput Assist Tomogr* 2016; **40**: 899–906. doi: <https://doi.org/10.1097/RCT.0000000000000450>
- Raghu G, Collard HR, Egan JJ, Martinez FJ, Behr J, Brown KK, et al. An official ATS/ERS/JRS/ALAT statement: idiopathic pulmonary fibrosis: evidence-based guidelines for diagnosis and management. *Am J Respir Crit Care Med* 2011; **183**: 788–824. doi: <https://doi.org/10.1164/rccm.2009-040GL>
- Block KT, Chandarana H, Milla S, Bruno M, Mulholland T, Fatterpekar G, et al. Towards routine clinical use of radial Stack-of-Stars 3D gradient-echo sequences for reducing motion sensitivity. *J Korean Soc Magn Reson Med* 2014; **18**: 87. doi: <https://doi.org/10.13104/jksmrm.2014.18.2.87>
- Winkelmann S, Schaeffter T, Koehler T, Eggers H, Doessel O. An optimal radial profile order based on the golden ratio for time-resolved MRI. *IEEE Trans Med Imaging* 2007; **26**: 68–76. doi: <https://doi.org/10.1109/TMI.2006.885337>
- Grimm R, Fürst S, Dregely I, Forman C, Hutter JM, Ziegler SI, et al. Self-gated radial MRI for respiratory motion compensation on hybrid PET/MR systems. *Med Image Comput Comput Assist Interv* 2013; **16**(Pt 3): 17–24. doi: https://doi.org/10.1007/978-3-642-40760-4_3
- Paul J, Divkovic E, Wundrak S, Bernhardt P, Rottbauer W, Neumann H, et al. High-Resolution respiratory self-gated golden angle cardiac MRI: comparison of self-gating methods in combination with k-t sparse sense. *Magn Reson Med* 2015; **73**: 292–8. doi: <https://doi.org/10.1002/mrm.25102>
- Bydder M, Larkman DJ, Hajnal JV. Combination of signals from array coils using image-based estimation of coil sensitivity profiles. *Magn Reson Med* 2002; **47**: 539–48. doi: <https://doi.org/10.1002/mrm.10092>
- Hansell DM, Bankier AA, MacMahon H, McLoud TC, Müller NL, Remy J. Fleischner Society: glossary of terms for thoracic imaging. *Radiology* 2008; **246**: 697–722. doi: <https://doi.org/10.1148/radiol.2462070712>
- Buzan MTA, Eichinger M, Kreuter M, Kauczor H-U, Herth FJ, Warth A, et al. T2 mapping of CT remodelling patterns in interstitial lung disease. *Eur Radiol* 2015; **25**: 3167–74. doi: <https://doi.org/10.1007/s00330-015-3751-y>
- Mirsadraee S, Tse M, Kershaw L, Semple S, Schembri N, Chin C, et al. T1 characteristics of interstitial pulmonary fibrosis on 3T MRI—a predictor of early interstitial change? *Quant Imaging Med Surg* 2016; **6**: 42–9. doi: <https://doi.org/10.3978/j.issn.2223-4292.2016.02.02>
- Cottin V, disease llung. Interstitial lung disease.. *Eur Respir Rev* 2013; **22**: 26–32. doi: <https://doi.org/10.1183/09059180.00006812>
- Takahashi M, Kunugi S, Terasaki Y, Terasaki M, Urushiyama H, Kuwahara N, et al. The difference of neovascularization in early intra-alveolar fibrosis between nonspecific interstitial pneumonia and usual interstitial pneumonia. *Pathol Int* 2013; **63**: 237–44. doi: <https://doi.org/10.1111/pin.12058>
- Wang JM, Robertson SH, Wang Z, He M, Virgincar RS, Schrank GM, et al. Using hyperpolarized ¹²⁹Xe MRI to quantify regional gas transfer in idiopathic pulmonary fibrosis. *Thorax* 2018; **73**: 21–8. doi: <https://doi.org/10.1136/thoraxjnl-2017-210070>
- Pierce IT, Keegan J, Drivas P, Gatehouse PD, Firmin DN. Free-breathing 3D late gadolinium enhancement imaging of the left ventricle using a stack of spirals at 3T. *J Magn Reson Imaging* 2015; **41**: 1030–7. doi: <https://doi.org/10.1002/jmri.24643>
- Jacob J, Bartholmai BJ, Rajagopalan S, Kokosi M, Nair A, Karwoski R, et al. Automated quantitative computed tomography versus visual computed tomography scoring in idiopathic pulmonary fibrosis: validation against pulmonary function. *J Thorac Imaging* 2016; **31**: 304–11. doi: <https://doi.org/10.1097/RTI.0000000000000220>
- Kreuter M, Bonella F, Wijsenbeek M, Maher TM, Spagnolo P. Pharmacological treatment of idiopathic pulmonary fibrosis: current approaches, unsolved issues, and future perspectives. *Biomed Res Int* 2015; **2015**: 1–10. doi: <https://doi.org/10.1155/2015/329481>
- Silva CIS, Müller NL, Pneumonias II. Idiopathic interstitial pneumonias.. *J Thorac Imaging* 2009; **24**: 260–73. doi: <https://doi.org/10.1097/RTI.0b013e3181c1a9eb>
- Yoshida S, Wu D, Fukumoto M, Akagi N, Seguchi H. Quantitative study of the difference in pulmonary perfusion in different respiratory phases in healthy volunteers. *Ann Nucl Med* 2002; **16**: 533–9. doi: <https://doi.org/10.1007/BF02988630>
- Feng L, Huang C, Shanbhogue K, Sodickson DK, Chandarana H, Otazo R. RACER-GRASP: Respiratory-weighted, aortic contrast enhancement-guided and coil-unstreaking golden-angle radial sparse MRI. *Magn Reson Med* 2018; **80**: 77–89. doi: <https://doi.org/10.1002/mrm.27002>
- Alhamad EH, Al-Boukai AA, Al-Kassimi FA, Alfaleh HF, Alshamiri MQ, Alzeer AH, et al. Prediction of pulmonary hypertension in patients with or without interstitial lung disease: reliability of CT findings. *Radiology* 2011; **260**: 875–83. doi: <https://doi.org/10.1148/radiol.11103532>